S=1 “QSL” in a Ni-based multilayer triangular system

Gang Chen
CU Boulder

- Motivation
- Theory
- Prediction

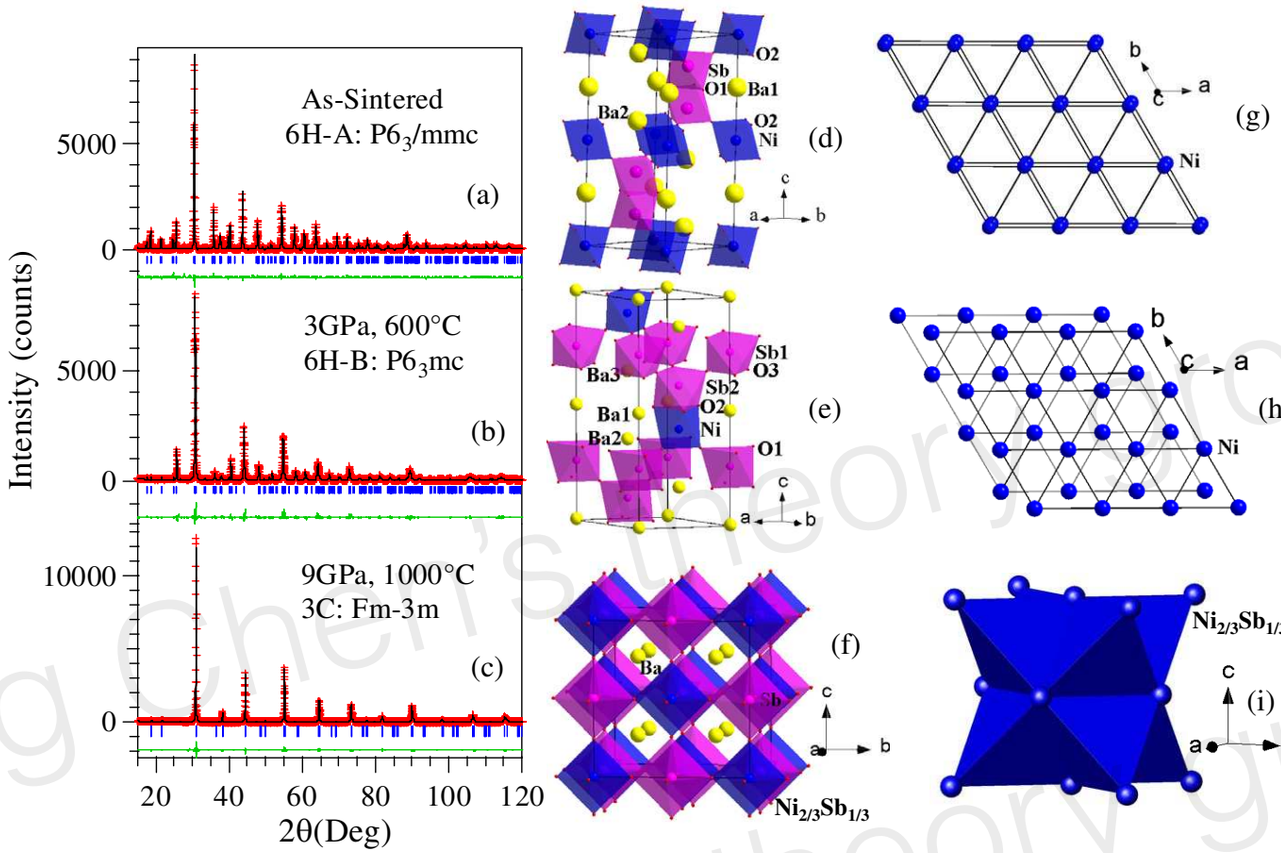

FIG. 1: (Color online) Powder XRD patterns (crosses) at 295 K for the $Ba_3NiSb_2O_9$ polytypes: (a) 6H-A, (b) 6H-B, and (c) 3C. Solid curves are the best fits obtained from Rietveld refinements using FullProf. Schematic crystal structures for the $Ba_3NiSb_2O_9$ polytypes: (d) 6H-A, (e) 6H-B, and (f) 3C, red octahedra represents Sb(M') site and blue octahedra represents $Ni_{2/3}Sb_{1/3}$(M) site. Magnetic lattices composed of Ni^{2+} ions for the $Ba_3NiSb_2O_9$ polytypes: (g) 6H-A, (h) 6H-B, and (i) 3C.

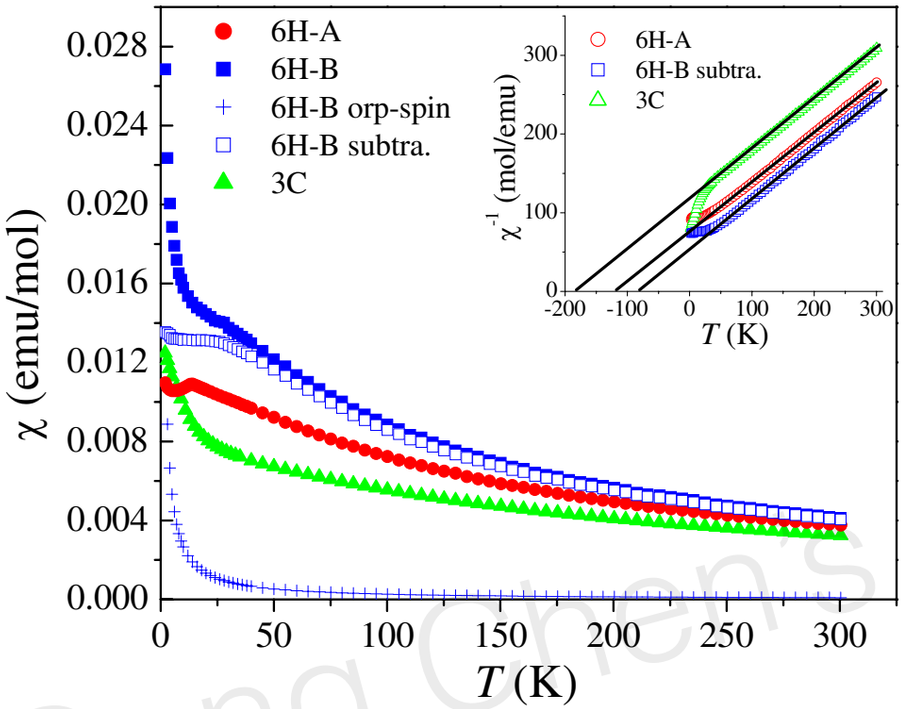

FIG. 2: (Color online) (a) Temperature dependencies of the DC magnetic susceptibility (χ) for the $Ba_3NiSb_2O_9$ polytypes. Inset: Temperature dependencies of $1/\chi$. The solid lines on $1/\chi$ data represent Curie-Weiss fits. For 6H-B phase, χ (open squares) is obtained by subtracting 1.7% Ni^{2+} orphan spin's contribution (crosses) from the as measured data (solid squares).

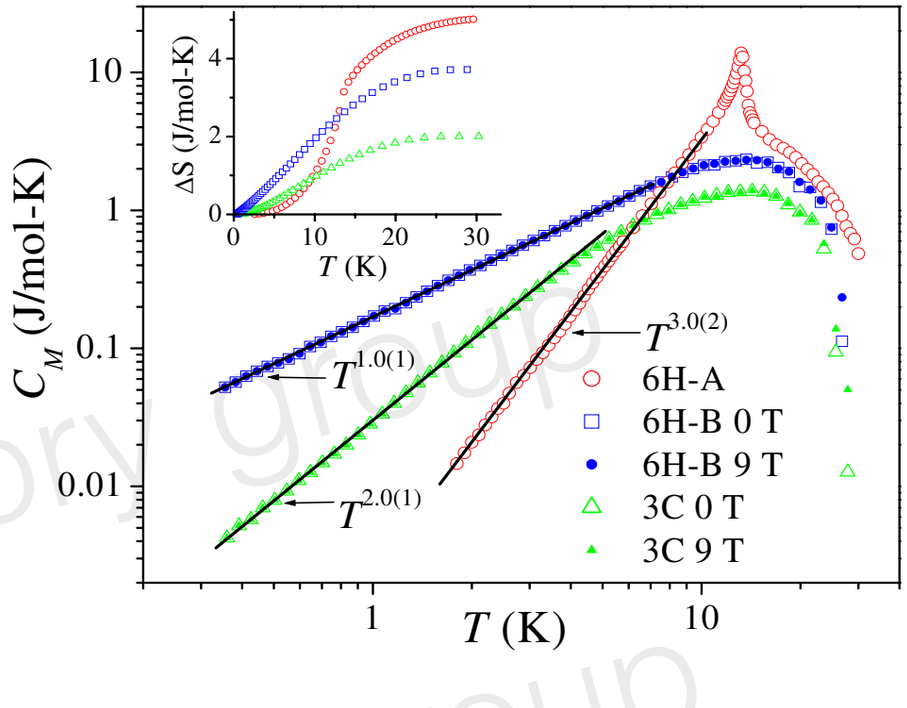

FIG. 3: (Color online) (a) Temperature dependencies for the magnetic specific heat (C_M) for all three $Ba_3NiSb_2O_9$ polytypes. Solid lines are the fits as described in the main text. Inset: variation in magnetic entropy ΔS below 30 K.

Works of other groups: I

$$H = \sum_{\langle ij \rangle} [J \vec{S}_i \cdot \vec{S}_j + K(\vec{S}_i \cdot \vec{S}_j)^2] + D \sum_i (S_i^z)^2,$$

$$\vec{S}_i = -\mathrm{i} \vec{f}_i^\dagger \times \vec{f}_i, \qquad \vec{f}_i^\dagger \cdot \vec{f}_i = 1.$$

$$|x\rangle = \mathrm{i}(|1\rangle - |-1\rangle)/\sqrt{2}$$

$$|y\rangle = (|1\rangle + |-1\rangle)/\sqrt{2}$$

$$|z\rangle = -\mathrm{i}|0\rangle$$

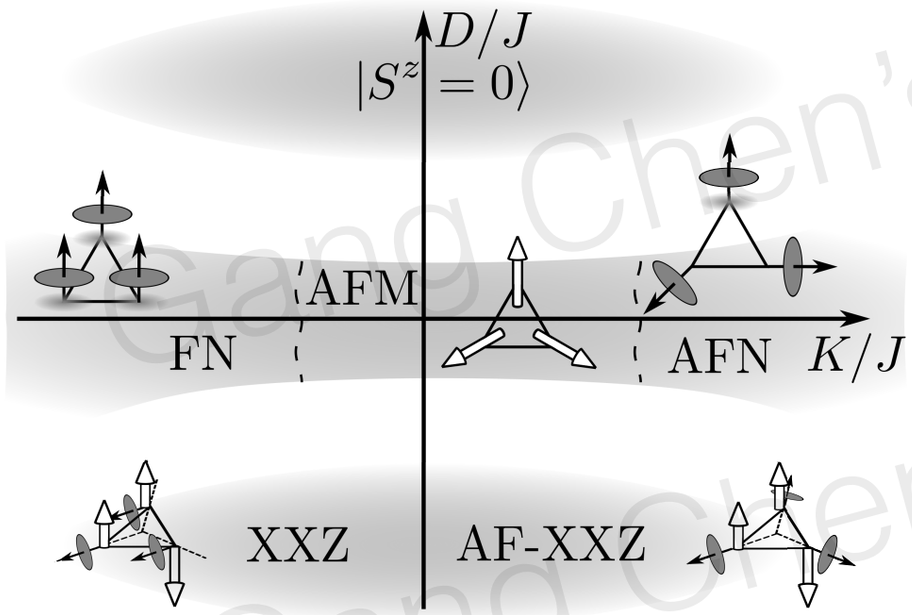

FIG. 1. Schematic representation of the ground state in different limits of the Hamiltonian (1). White arrows represent average spin; arrows with discs indicate the director of the nematic order parameter. Details are discussed in the text.

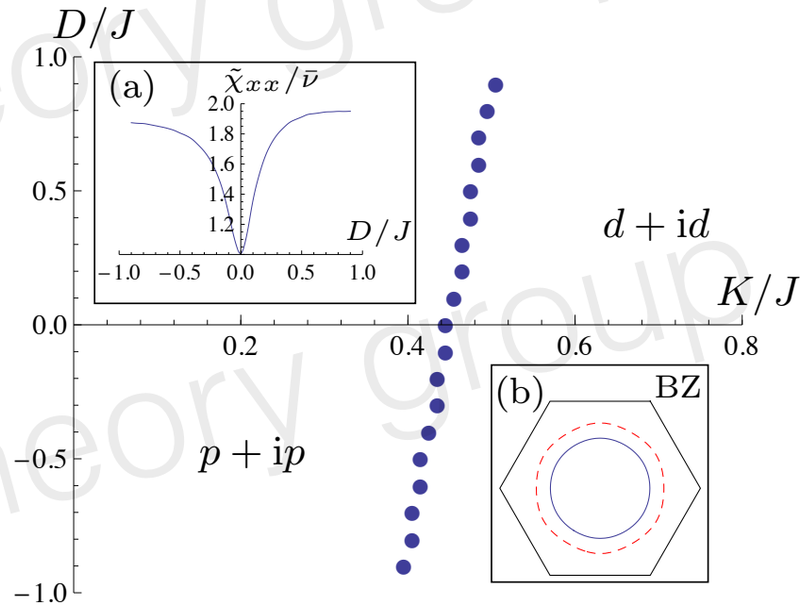

FIG. 2. The phase boundary between SL GS's with $p+\mathrm{i}p$ and $d+\mathrm{i}d$ pairing. (a) The spin susceptibility $\tilde{\chi}_{xx}$ in the $d+\mathrm{i}d$ phase as a function of D/J for $K/J = 0.55$. The susceptibility is normalized by the average density of states, $\bar{\nu} = (\nu_x + \nu_z)/2$, where ν_x is calculated without the gap. (b) Gapped (dashed red line) and ungapped (blue line) Fermi surfaces of x, y, and z-fermions for $K/J = 0.55$, $D/J = 0.8$.

ArXiv 1108.3070

Works of other groups: II

$$\hat{S}_i^\mu = \frac{1}{2} \sum_{\alpha,\beta=\uparrow,\downarrow} \sum_{a=1,2} f^\dagger_{\alpha,a,i} \sigma^\mu_{\alpha\beta} f_{\beta,a,i}.$$

$$\hat{n}_i = \sum_{a=1,2} \sum_{\alpha=\uparrow,\downarrow} f^\dagger_{\alpha,a,i} f_{\alpha,a,i} = 2,$$

$$\hat{\tau}^\mu = \sum_{\alpha,a,b} f^\dagger_{\alpha,a,i} \tau^\mu_{ab} f_{\alpha,b,i} = 0.$$

$$\mathrm{U}(1)_c \ : \ f_{\alpha,a,i} \to e^{i\theta_i} f_{\alpha,a,i};$$

$$\mathrm{SU}(2)_o \ : \ f_{\alpha,a,i} \to [e^{i\vec{\theta}_i \cdot \vec{\tau}/2}]_{ab} f_{\alpha,b,i}.$$

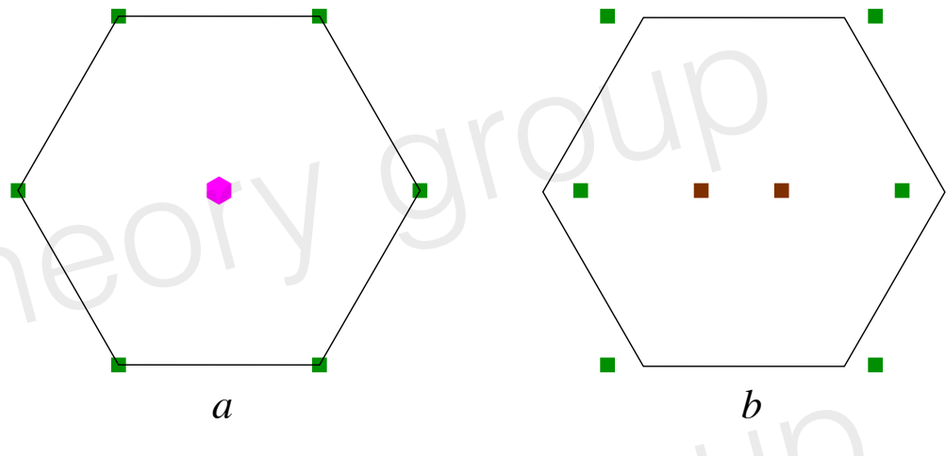

FIG. 1: a, The spin liquid we are considering contains a quadratic band touching at $\vec{k} = 0$ (hexagon), and Dirac points (squares) at the corners of the Brillouin zone. b, with a nonzero and small nematic order $N_1 > 0$, the quadratic band touching is split into two Dirac points, and the locations of the other Dirac points are shifted.

ArXiv 1110.3328

Crystal structure

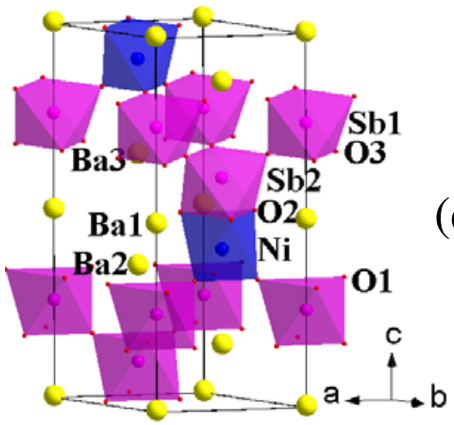

(e)

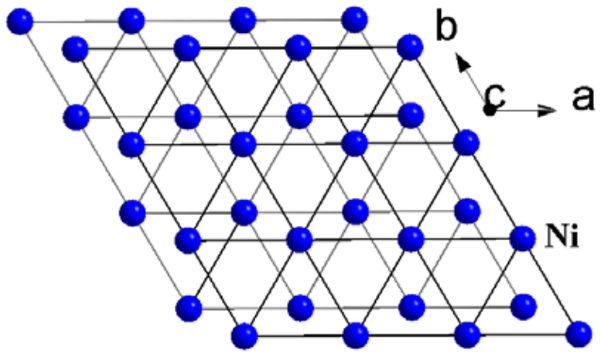

(h)

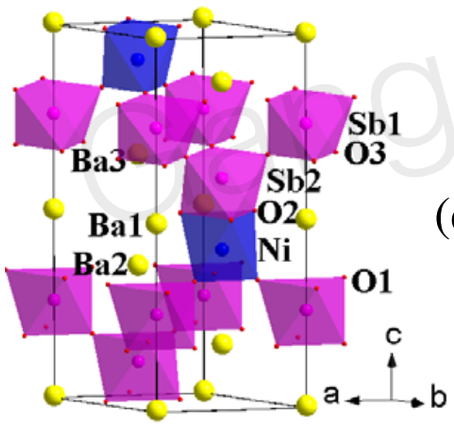

(e)

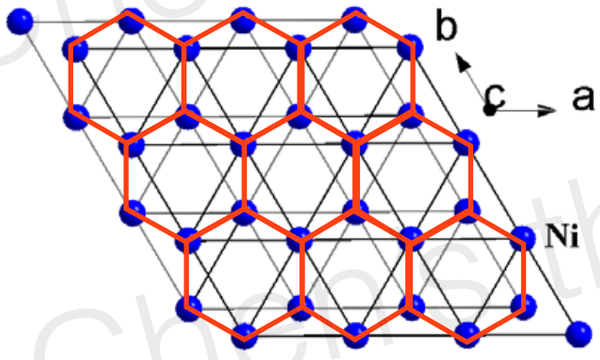

(h)

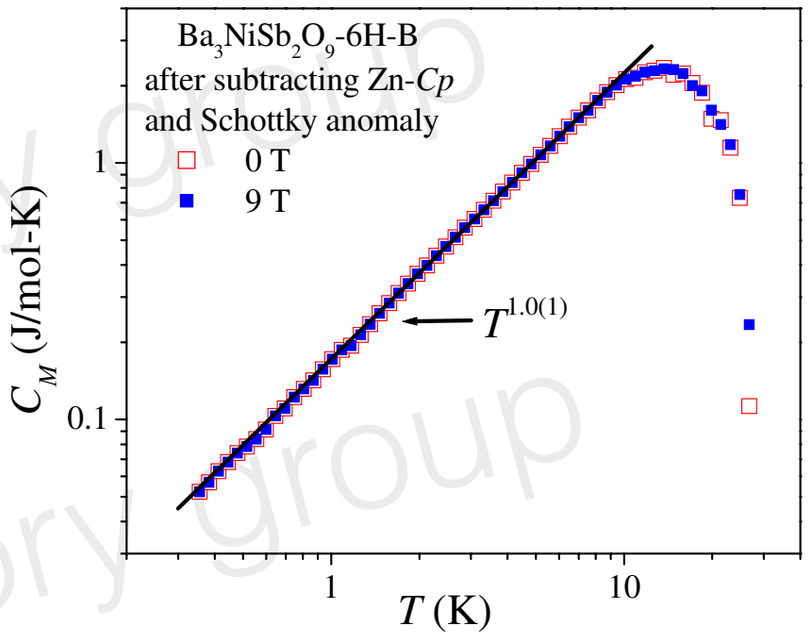

$$\mu_{\text{eff}} \sim 3.54\ \mu_B$$

$$\Theta_{CW} = -75.6K$$

Model

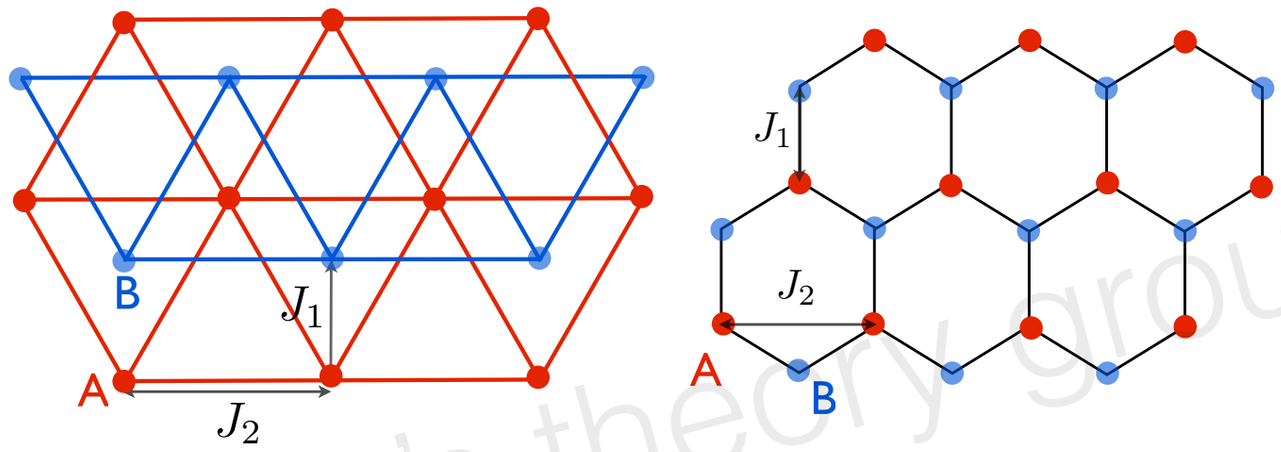

FIG. 1. (Color online) The bilayer triangular lattice (on left) is equivalent to a single layer honeycomb lattice (on right). A (in dark red) and B (in light blue) denote two triangular latttice (on left) or two sublattices of honeycomb lattice (on right). J_1, J_2 are interlayer and intralayer exchange, respectively.

$$\mathcal{H}_{\text{ex}} = J_1 \sum_{\langle ij\rangle \in \text{AB}} \mathbf{S}_i \cdot \mathbf{S}_j + J_2 \sum_{\langle ij\rangle \in \text{AA or BB}} \mathbf{S}_i \cdot \mathbf{S}_j,$$

$$\mathcal{H}_{\text{ani}} = D \sum_i (S_i^z)^2,$$

Phase diagram

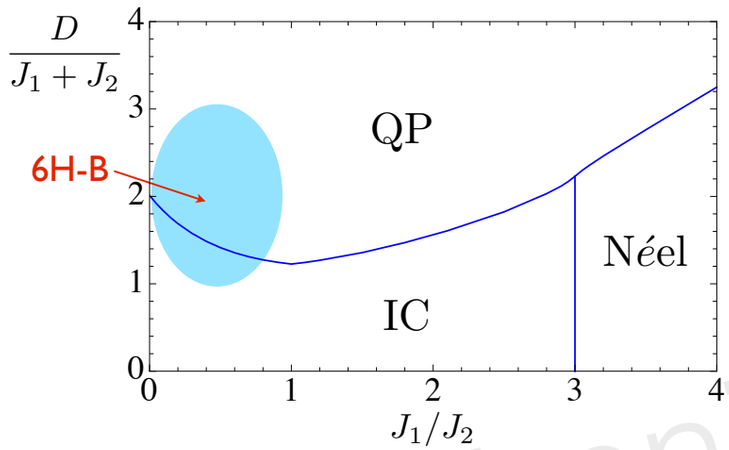

FIG. 2. (Color online) Zero temperature phase diagram determined from the SPE. In the figure, "IC"=incommensurate spin order, "Néel"= Néel state, "QP"=quantum paramagnet. Shaded region (in blue) is the expected parameter regime for the 6H-B compound.

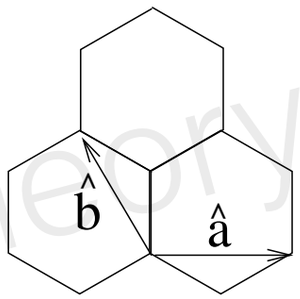

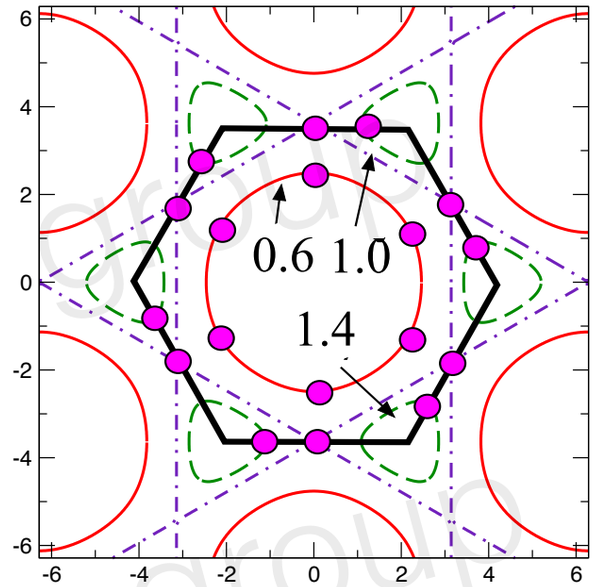

$$\sum_{\{\mathbf{b}\}} \cos(\mathbf{q}_\perp \cdot \mathbf{b}) = (\frac{J_1}{J_2})^2 - 3,$$

Quantum order-by-disorder

$$\mathbf{q}_\perp = \left(0, \frac{2}{\sqrt{3}} \cos^{-1}\left((\frac{J_1}{2J_2})^2 - \frac{5}{4}\right)\right), \text{ if } 1 < \frac{J_1}{J_2} < 3$$

$$\mathbf{q}_\perp = \left(2\cos^{-1}(\frac{J_1}{2J_2} + \frac{1}{2}), \frac{2\pi}{\sqrt{3}}\right), \qquad \text{if } \frac{J_1}{J_2} < 1,$$

MFT:I

$$\mathbf{S}_{\mathrm{A}}(\mathbf{r}) = M[\cos(\mathbf{q}\cdot\mathbf{r})\hat{x} + \sin(\mathbf{q}\cdot\mathbf{r})\hat{y}],$$
$$\mathbf{S}_{\mathrm{B}}(\mathbf{r}) = M[\cos(\mathbf{q}\cdot\mathbf{r}+\phi)\hat{x} + \sin(\mathbf{q}\cdot\mathbf{r}+\phi)\hat{y}].$$

$$M = \sqrt{2(1 - D/D_c)}$$

$$\chi^{\perp}(T\to 0) = \frac{2\mu_0(g\mu_B)^2}{D + 12J_1 + 12J_2}.$$

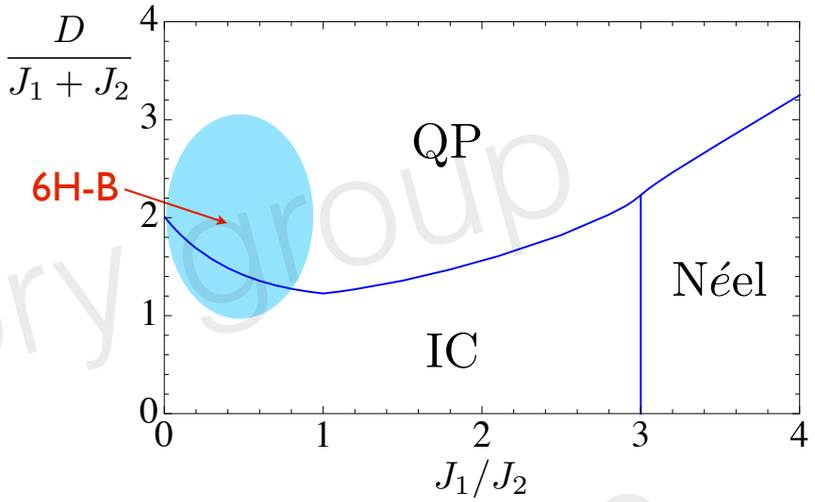

FIG. 2. (Color online) Zero temperature phase diagram determined from the SPE. In the figure, "IC"=incommensurate spin order, "Néel"= Néel state, "QP"=quantum paramagnet. Shaded region (in blue) is the expected parameter regime for the 6H-B compound.

MFT:II

Map to rotor model

$$S_i^z \to n_i \text{ and } S_i^+ \to \sqrt{2}e^{i\phi_i}, \qquad [\phi_i, n_j] = i\delta_{ij}.$$

$$\mathcal{H}_{\text{rotor}} = \frac{1}{2}\sum_{ij} J_{ij}[2\cos(\phi_i - \phi_j) + n_i n_j] + \sum_i D n_i^2.$$

$$\mathcal{Z} = \int \mathcal{D}\Phi \prod_i \delta(|\Phi_i|^2 - 1) e^{-S} \qquad (11)$$

with

$$\mathcal{S} = \int_\tau \sum_{\mathbf{k}} (4D\mathbb{I} + 2\mathcal{J}_{\mathbf{k}})^{-1}_{\mu\nu} \partial_\tau \Phi^*_{\mu,\mathbf{k}} \partial_\tau \Phi_{\nu,-\mathbf{k}} + \sum_{ij} J_{ij} \Phi_i^* \Phi_j$$

$$s_\pm(\mathbf{k}) = \sum_{\{\mathbf{b}\}} J_2 \cos(\mathbf{k}\cdot\mathbf{b}) \pm |J_1(1 + e^{ik_z}) \sum_{\{\mathbf{a}\}} e^{i\mathbf{k}\cdot\mathbf{a}}|$$

$$\Rightarrow \quad \mathcal{Z} = \int \mathcal{D}\Phi\mathcal{D}\lambda\, e^{-S - i\sum_i \lambda_i(|\Phi_i|^2 - 1)}.$$

Saddle-point equation

$$\sum_{i=\pm} \int_{\mathbf{k}} \frac{2D + s_i(\mathbf{k})}{\epsilon_i(\mathbf{k})} \coth(\beta\epsilon_i(\mathbf{k})/2) = 2,$$

$$\epsilon_\pm(\mathbf{k}) = \sqrt{(4D + 2s_\pm(\mathbf{k}))(\Delta(T) + s_\pm(\mathbf{k}))}.$$

$$i\lambda_i = \beta\Delta(T)$$

MFT:II

Map to rotor model

$$S_i^z \to n_i \text{ and } S_i^+ \to \sqrt{2}e^{i\phi_i}, \qquad [\phi_i, n_j] = i\delta_{ij}.$$

$$\mathcal{H}_{\text{rotor}} = \frac{1}{2}\sum_{ij} J_{ij}[2\cos(\phi_i - \phi_j) + n_i n_j] + \sum_i D n_i^2.$$

$$\mathcal{Z} = \int \mathcal{D}\Phi \prod_i \delta(|\Phi_i|^2 - 1) e^{-S} \qquad (11)$$

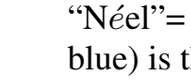

$$\mathcal{Z} = \int \mathcal{D}\Phi \mathcal{D}\lambda\, e^{-S - i\sum_i \lambda_i (|\Phi_i|^2 - 1)}.$$

with

$$\mathcal{S} = \int_\tau \sum_{\mathbf{k}} (4D\mathbb{I} + 2\mathcal{J}_{\mathbf{k}})^{-1}_{\mu\nu} \partial_\tau \Phi^*_{\mu,\mathbf{k}} \partial_\tau \Phi_{\nu,-\mathbf{k}} + \sum_{ij} J_{ij} \Phi_i^* \Phi_j$$

$$s_\pm(\mathbf{k}) = \sum_{\{\mathbf{b}\}} J_2 \cos(\mathbf{k}\cdot\mathbf{b}) \pm |J_1(1 + e^{ik_z}) \sum_{\{\mathbf{a}\}} e^{i\mathbf{k}\cdot\mathbf{a}}|$$

Saddle-point equation

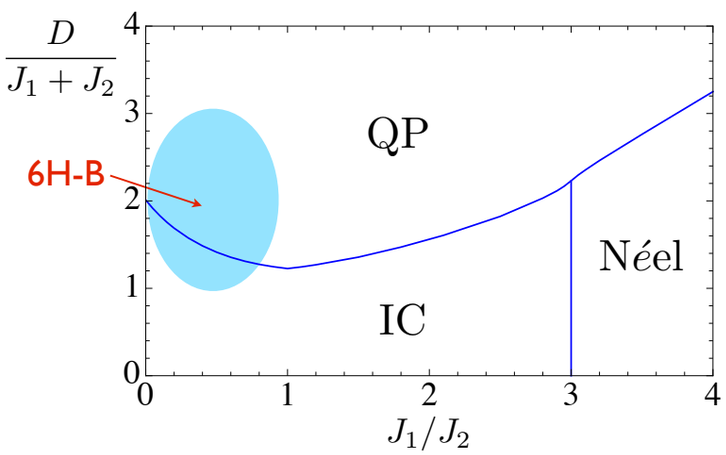

FIG. 2. (Color online) Zero temperature phase diagram determined from the SPE. In the figure, "IC"=incommensurate spin order, "Néel"= Néel state, "QP"=quantum paramagnet. Shaded region (in blue) is the expected parameter regime for the 6H-B compound.

Low-E spin excitation

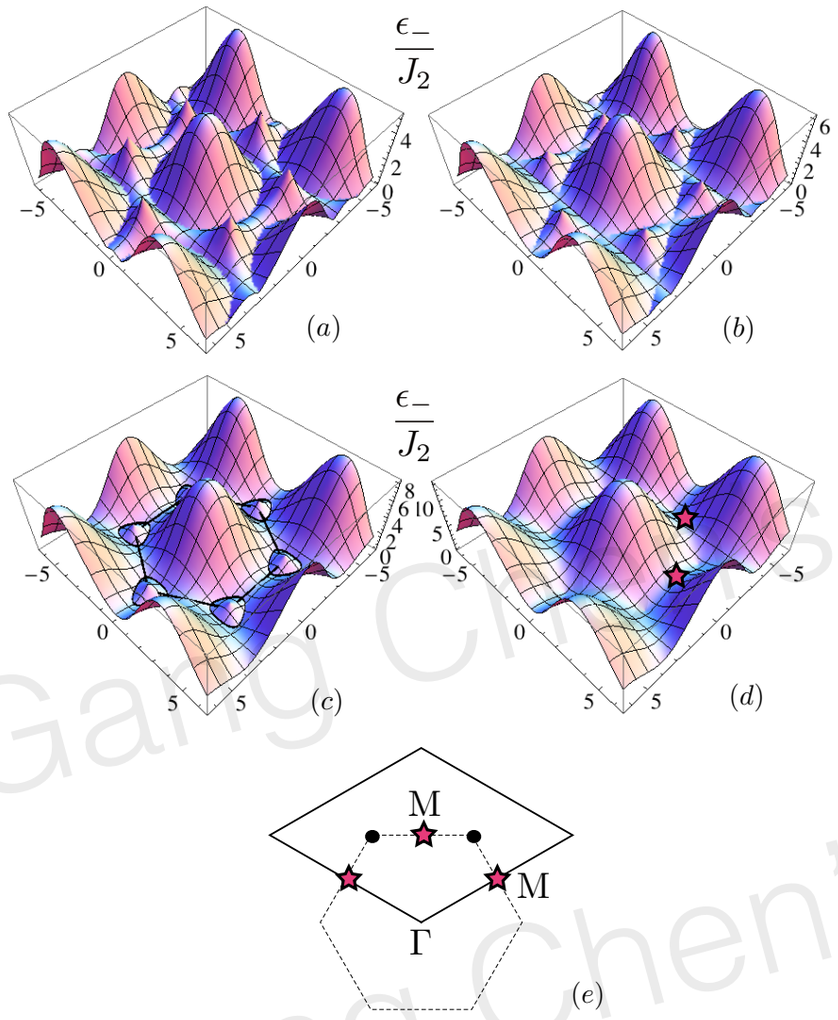

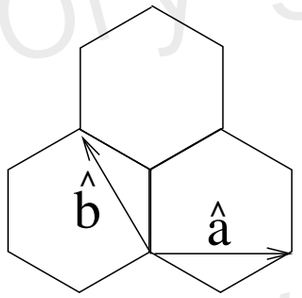

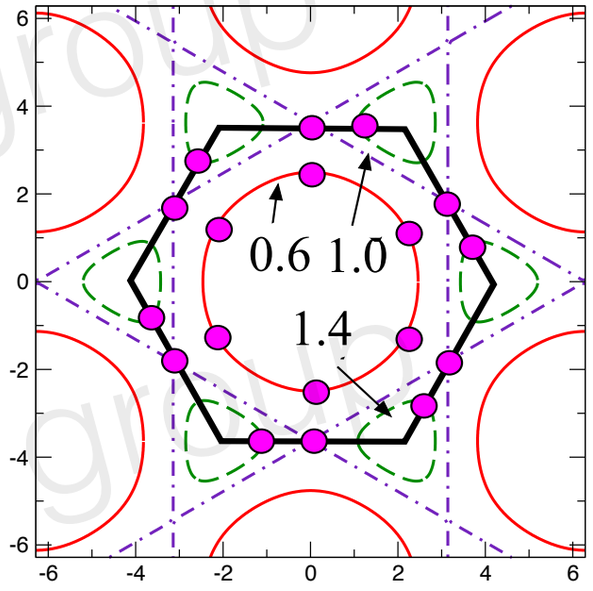

FIG. 3. (Color online) The evolution of the low-energy spin excitations in k_x-k_y plane with $k_z = 0$ at the QCP. (a) $J_1 = 1.2J_2, D_c = 2.79J_2$, (b) $J_1 = J_2, D_c = 2.456J_2$, (c) $J_1 = 0.7J_2, D_c = 2.33J_2$, (d) $J_1 = 0, D_c = 2.01J_2$. Lattice constants in xy plane are set to be 1. (e) and the hexagon in (c) is the Brillouin zone (BZ) of the honeycomb lattice. When $J_1 > J_2$, the nodal line is centered in the middle of BZ. When $J_1 < J_2$, the nodal lines are centered around and eventually shrink to the corners of BZ in the limit $J_1 \to 0$. The "★" in (d) and (e) indicates the locations of the momenta with energy scale Λ_c (see the text).

Finite-T specific heat

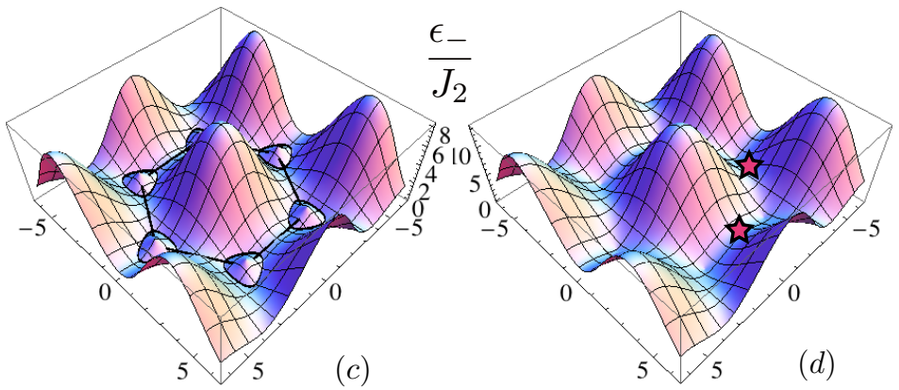

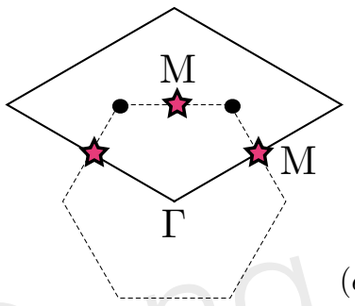

(e)

$$\Lambda_c \simeq 2\sqrt{J_2(D-J_2)}$$

For $\epsilon_\pm < \lambda\Lambda_c$

$$\epsilon_\pm(\mathbf{q}) \simeq \sqrt{A\Delta_1(T) + v^2\mathbf{q}^2}$$

$$v^2 \approx 3DJ_2 - 9J_2^2/2.$$

$$A = 4D_c - 2\Delta_0.$$

$$\Delta(T) = \Delta_0 + \Delta_1(T)$$

Saddle-point equation $\sum_{i=\pm}\int_{\mathbf{k}} \frac{2D + s_i(\mathbf{k})}{\epsilon_i(\mathbf{k})} \coth(\beta\epsilon_i(\mathbf{k})/2) = 2,$

$$4\pi A \int_{\mathbf{q}}^{\lambda\Lambda_c} \frac{\coth(\beta\sqrt{A\Delta_1(T) + v^2\mathbf{q}^2}/2)}{\sqrt{A\Delta_1(T) + v^2\mathbf{q}^2}} + \text{const} = 2,$$

$$f\left(\frac{T}{\lambda\Lambda_c}, \frac{A\Delta_1(T)}{T^2}\right)$$

$$\Delta_1(T) \simeq cT^2$$

$T \ll \lambda\Lambda_c$

$$E \sim 8\pi \int_{\mathbf{q}} \frac{\sqrt{cAT^2 + v^2\mathbf{q}^2}}{e^{\beta\sqrt{cAT^2+v^2\mathbf{q}^2}} - 1} \propto T^2$$

Unscaled

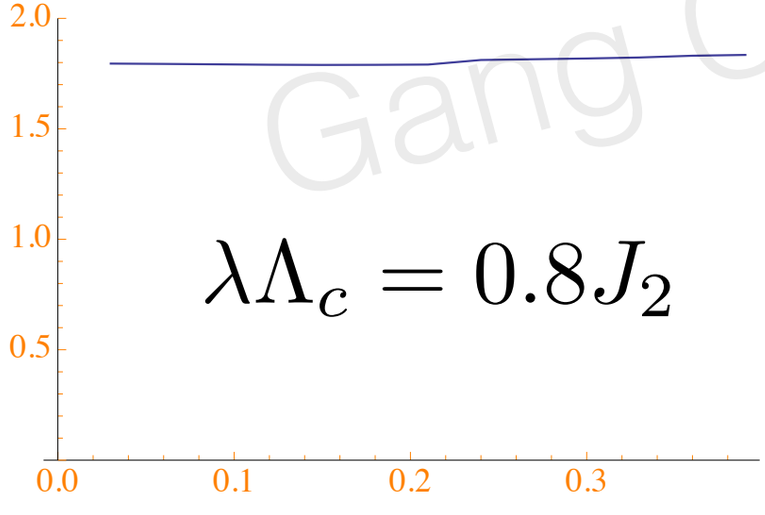

$$\lambda\Lambda_c = 0.8J_2$$

Specific heat

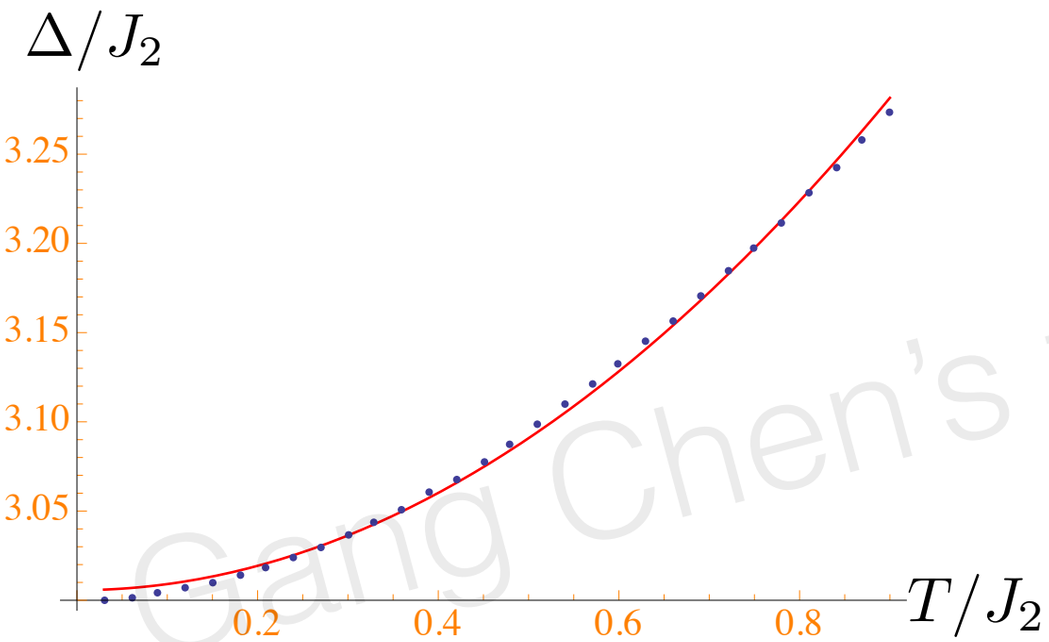

$$J_1 = 0, \quad D_c = 2.01 J_2$$

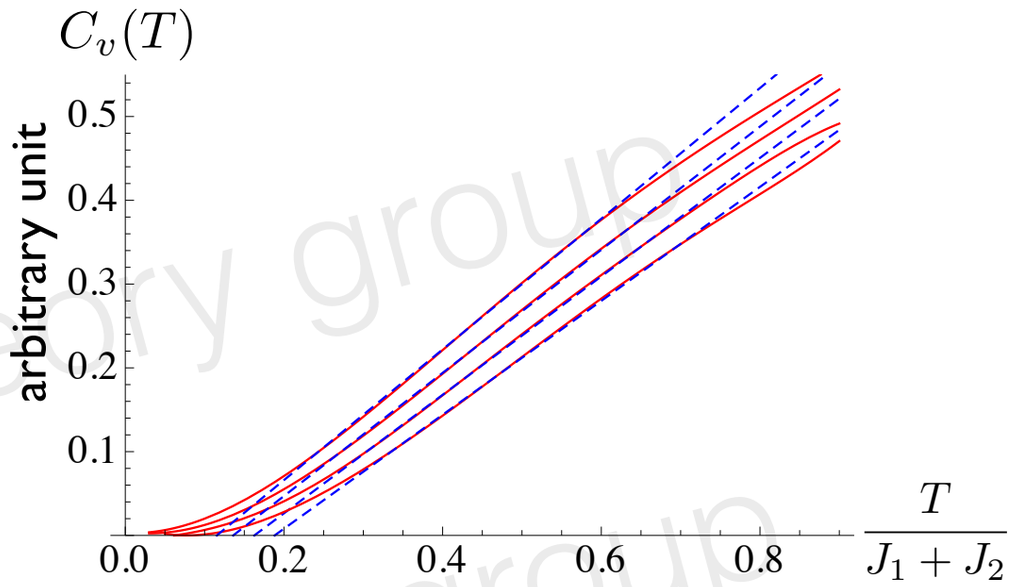

FIG. 4. (Color online) The temperature dependence of specific heat. In the plot, $J_1 = 0.15 J_2$. The critical $D_c = 2.018 J_2$. For the curves in the plot, from top to bottom $D = 2.02 J_2, 2.12 J_2, 2.22 J_2, 2.32 J_2$. The dash lines are the linear fit for a range of data points.

Other prediction

1. NMR

2. Neutron scattering

3. Crossover

Spin Liquid State in the $S = 1/2$ Triangular Lattice $Ba_3CuSb_2O_9$

H. D. Zhou,[1,*] E. S. Choi,[1] G. Li,[1] L. Balicas,[1] C. R. Wiebe,[1,2,3] Y. Qiu,[4,5] J. R. D. Copley,[4] and J. S. Gardner[4,6]

[1]*National High Magnetic Field Laboratory, Florida State University, Tallahassee, Florida 32306-4005, USA*
[2]*Department of Chemistry, University of Winnipeg, Winnipeg, MB, R3B 2E9 Canada*
[3]*Department of Chemistry, University of Manitoba, Winnipeg, MB, R3T 2N2 Canada*
[4]*NIST Center for Neutron Research, Gaithersburg, Maryland, 20899-6102, USA*
[5]*Department of Materials Science and Engineering, University of Maryland, College Park, Maryland, 20742, USA*
[6]*Indiana University, 2401 Milo B. Sampson Lane, Bloomington, Indiana 47408, USA*

(Received 12 October 2010; published 6 April 2011)

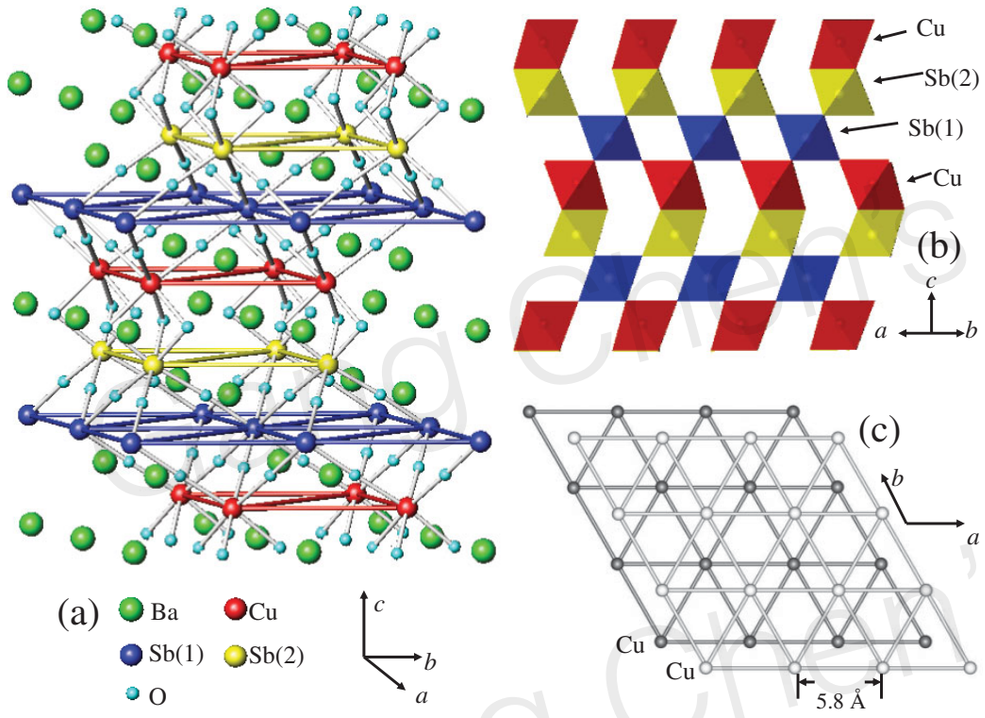

FIG. 1 (color). (a) Schematic crystal structure for $Ba_3CuSb_2O_9$; (b) The layer structure along the c axis; (c) The triangular lattice of Cu^{2+} in the ab plane.

$$g = 2.07$$

$$\theta_{\mathrm{CW}} = -55\ \mathrm{K}$$

$$z = 6,\ J/k_B = -2/3\theta_{\mathrm{CW}} = 37\ \mathrm{K},$$

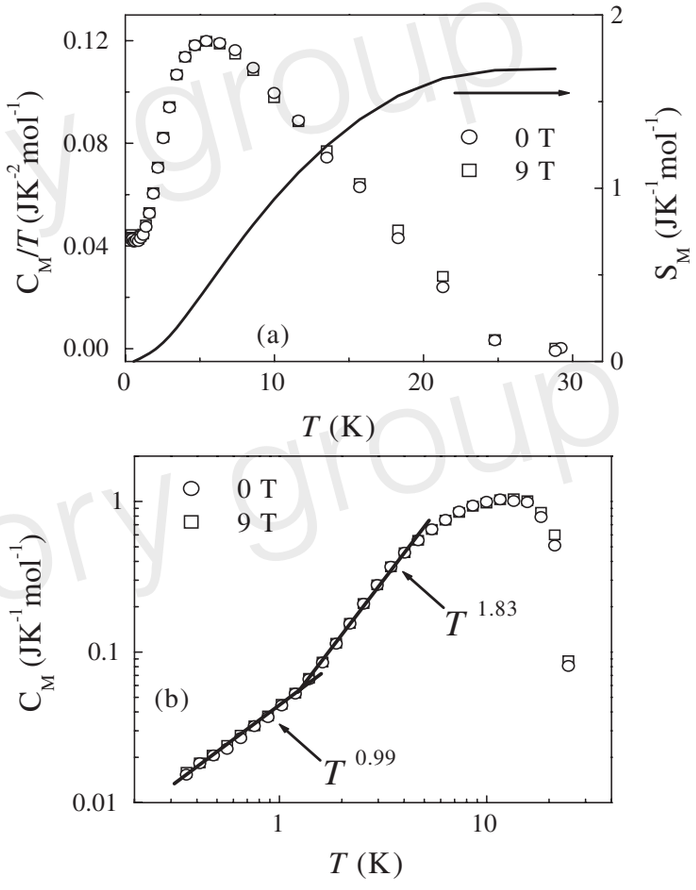

FIG. 4. (a) The temperature dependencies of C_M/T and the magnetic entropy variation S_M. (b) The temperature dependence of C_M (open symbols). The solid lines are fits as described in the text.

Spiral spin liquid?

Summary

1. we study the spin-1 multilayer triangular lattice magnet.

2. we propose the quantum criticality to be the origin of the puzzling spin liquid phenomena in Ni spin-1 magnet.